Monitoring interannual dynamics of desertification in Minqin County, China, using dense Landsat time series

Minqin County in northwestern China is highly affected by desertification. Campaigns have been initiated in recent decades to combat desertification in Minqin. To assess the effectiveness of these campaigns, this study used dense Landsat time series from 1987 to 2017 to investigate the interannual dynamics of vegetation coverage and greenness over the past 31 years. First, this study applied an advanced technology to reconstruct a high-quality Landsat annual time series. Specifically, one image in the vegetation-peak season was selected as the base image in each year, and then problematic pixels were interpolated by the neighborhood similar pixel interpolator using ancillary images in the same year. Second, the land cover map and the enhanced vegetation index (EVI) were derived from all reconstructed images. Third, the change of vegetation coverage and EVI values over the 31 years were analyzed. The results show that the total vegetation coverage and greenness increased during the 31 years. Linking this change trend to other factors suggests that vegetation in Minqin County is highly affected by agriculture and groundwater supply rather than by climate. To mitigate desertification in a sustainable way, agriculture should be well managed to avoid overconsumption of natural resources such as underground water.

Keywords: Minqin County; desertification; agriculture; Landsat; time series; vegetation cover

Introduction

Desertification indicates land degradation and conversion to drylands (Zucca et al., 2011). Currently, deserts occupy approximately 40% of the global land area, and desertification affects more than 1 billion people around the world (Tang et al., 2016). China is one of the countries facing serious desertification. By 2014, desertified lands consist of 2.61 million km^2, accounting for 27.2% of the total land of China (Feng et al., 2016), and 99.6% of these deserts are located in north and northwest China (Zhou et al., 2015). Northwest China has most of the deserts of China and is the origin of sandstorms in China (Wang et al., 2004). Northwest China still faces the threat of desertification. Over 90% of the grassland in the region has suffered different degrees of land degradation (Zhou et al., 2015).

The Chinese government has expressed high concern for slowing down desertification. The government enacted the Law of Combating Desertification in 2002 and approved the National Plan for Combating Desertification in 2005. In addition, the government has launched several national ecological engineering projects such as the Three-North Shelterbelt Project (from 1978 to present) and Beijing and Tianjin Sandstorm Source Treatment Project (from 2001 to 2010) (Wang et al., 2013). Since the Chinese government has been combating desertification in recent decades, it is urgent to monitor the interannual dynamics of vegetation to know whether these actions have been effective or not.

Due to the moderate spatial resolution and free data policy, Landsat images are widely used to detect land cover change on the regional scale, and several studies have attempted to use Landsat images for monitoring the desertification process in China. For example, using Landsat images from the years 1986 and 2000, Guo and Li (2005) monitored and identified three types of sandy desertification of Minqin County. Sun and Liu (2015) proposed a multiseasonal linear spectral mixture analysis method for classifying the cover of vegetation, sand, saline land, and dark materials in Minqin County from Landsat images collected in three seasons in 2008. Subsequently, Sun (2015) applied this method to Landsat images collected in 2002 and 2008 and found that the water resources are the key element of the desertification syndrome in the dryland oasis. With Landsat images from the years 1991 and 2009, Wang et al. (2016) extracted the land cover change from these two periods and found a reduction of deserts. Although these studies tried to identify the desertification process and the driving forces of desertification using remote sensing data, we cannot evaluate the effectiveness of policies for protecting the vegetation because of two limitations. First, the monitoring period in existing studies is relatively short (e.g., 7 years in Sun (2015); 15 years in Guo and Li (2015); 19 years in Wang et al. (2016)), which cannot reveal the long-term effect of policies against desertification. Second, the time interval of these studies is too wide. Two images were typically used to infer the desertification process across the whole study period, which cannot capture the interannual dynamics of desertification.

The aim of this study is to address these limitations of existing studies and evaluate interannual dynamics of desertification in northwest China. To this end, first, a cloud-and gap-free Landsat image in vegetation peak season per year from 1987 to 2017 was reconstructed. Then, vegetation covers and greenness from Landsat images were extracted from these reconstructed images. Finally, the spatial and temporal pattern of vegetation change over the past 31 years was analyzed. This study provides a paradigm of studying desertification using long-term available historical Landsat images.

Study Area and Data

Minqin County, located in northwest China, was selected as the study area (Figure 1). This area has become one of China's most severely desertified regions over the last several decades. The size of the study area is 8,143 km^2. The study area has an arid climate. The average annual precipitation is 115 mm, but the average annual evaporation is as high as 2644 mm (Li, 2016). The precipitation is concentrated in May to August, with large annual variations. Minqin County has a long sunshine duration and frost-free period of 3073.5 hours and 162 days per year. Only 6% of the area of the county is suitable for agriculture, and farmland is spatially distributed along the streams and channels (Sun et al., 2005). Minqin County is surrounded by two deserts: Tengger Desert and Badain Jaran Desert. Minqin County is considered the green barrier to prevent the convergence of the Tengger Desert and the Badain Jaran Desert. Central and local government took measures to protect the land from further desertification. For example, the Grain to Green Program (GTGP) has saved 516,000 m^3 of water in 2003 through reducing irrigation on 4300 ha of the land in Minqin County (Liu et al., 2008). This area was selected as the study site because it is not only good for monitoring the environmental change and the corresponding impact but also good for assessing the effectiveness of government policies.

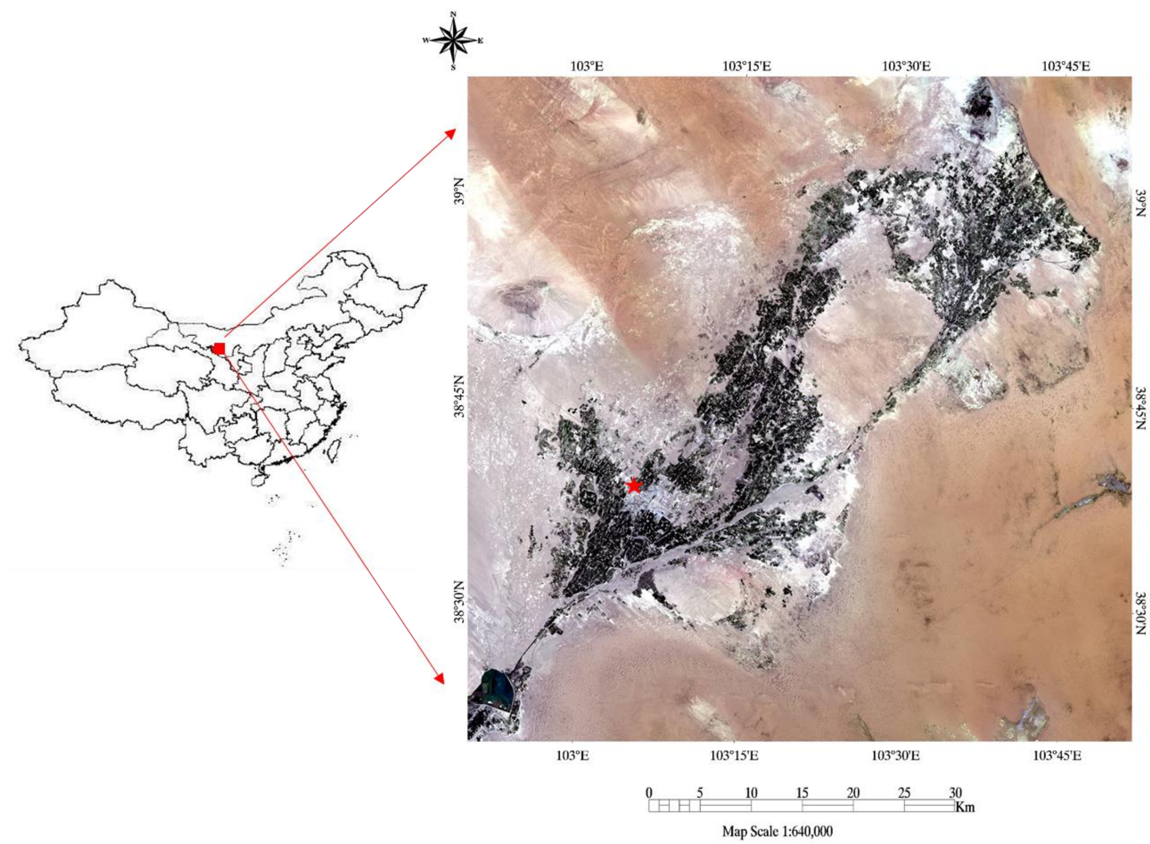

Figure 1. Study area of Minqin County shown by a true color Landsat image in 2017 (Red star: the location of the weather station in Minqin County)

In each year, one Landsat image with minimal cloud cover (and missing pixels for Landsat-7 ETM+ images after 2003) during the vegetation peak season was selected as the base image. Through inspecting the seasonality of the Advanced very-high-resolution radiometer (AVHRR) Normalized Difference Vegetation Index (NDVI) curve over the study area (Figure 2, data were extracted from Google Earth Engine), the vegetation peak season is from June to September. The AVHRR NDVI curve was used to define the vegetation peak season because AVHRR has very high temporal resolution to obtain a reliable temporal profile of vegetation growth. Table 1 lists the base Landsat image selected for each year, including the file names, dates, and the percentage of problematic pixels (including clouds, cloud shadows, and ETM+ gaps) derived from their quality flag mask. Some manual edits were done to correct errors in the quality flag mask. All the Landsat images used in this study were downloaded from Google Earth Engine and USGS Earth Explorer.

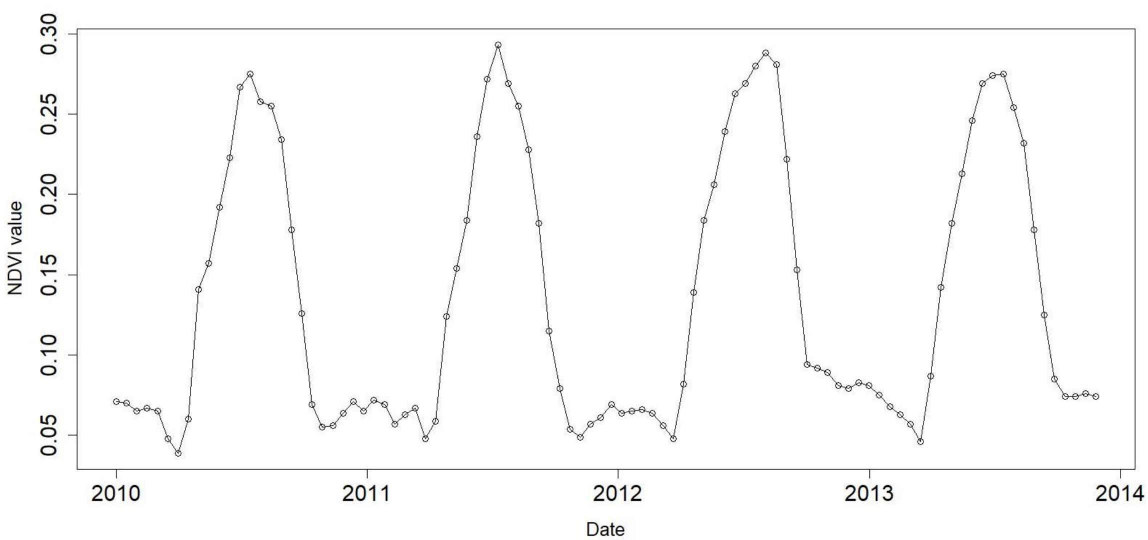

Figure 2. Advanced very-high-resolution radiometer (AVHRR) Normalized Difference Vegetation Index (NDVI) time series averaged over study area from 2010 to 2014 (data were extracted from Google Earth Engine)

Table 1. Base Landsat images selected for each year

Image file name	Date	Percentage of problematic pixels (%)
LT51310331987261BJC00	September 18, 1987	2.298
LT51310331988184BJC01	July 2, 1988	0.0523
LT51310331989266BJC01	September 23, 1989	0
LT51310331990173BJC00	June 22, 1990	0.0153
LT51310331991240BJC00	August 28, 1991	0
LT51310341992211BJC02	July 29, 1992	0
LT51310341993245BJC00	September 2, 1993	0.5664
LT51310341994200BJC00	July 19, 1994	0
LT51310331995187BJC00	July 6, 1995	0.0244
LT51310341996270BJC00	September 26, 1996	5.4515
LT51310331997224BJC00	August 12, 1997	2.9014
LT51310331998243BJC00	August 31, 1998	0.8625
LT51310331999214BJC00	August 2, 1999	0
LT51310332000201BJC00	July 19, 2000	1.976
LT51310332001203BJC00	July 22, 2001	0
LE71310332002198SGS00	July 17, 2002	4.8964
LT51310332003257BJC00	September 14, 2003	0
LE71310332004188SGS01	July 6, 2004	14.9778
LE71310332005158PFS00	June 7, 2005	22.0372
LE71310332006177PFS00	June 26, 2006	20.9881
LE71310332007196PFS00	July 15, 2007	20.1985
LE71310332008183PFS00	July 1, 2008	21.0963
LE71310342009265EDC00	September 22, 2009	20.8056
LE71310332010204PFS00	July 23, 2010	7.8123
LE71310332011175SGS00	June 24, 2011	21.321
LE71310342012242EDC00	August 29, 2012	22.557
LC81310332013156LGN00	June 5, 2013	7.8156
LC81310332014191LGN00	July 10, 2014	0
LC81310332015226LGN00	August 14, 2015	0
LC81310342016213LGN00	July 31, 2016	0
LC81310332017167LGN00	June 16, 2017	0.5852

Methodology

Figure 3 shows the flowchart of this study. The first step is reconstructing the high-quality (i.e., cloud- and gap-free) annual time series of Landsat images. Then, the reconstructed images are classified by supervised classifier to obtain the land cover map per year. The accuracy of classification is assessed using reference ground data. Following the classification, enhanced vegetation index (EVI) values are calculated from images in each year. The last step is analyzing the spatial and temporal pattern of vegetation change, including the cover change and greenness change, and exploring the possible reasons for these changes.

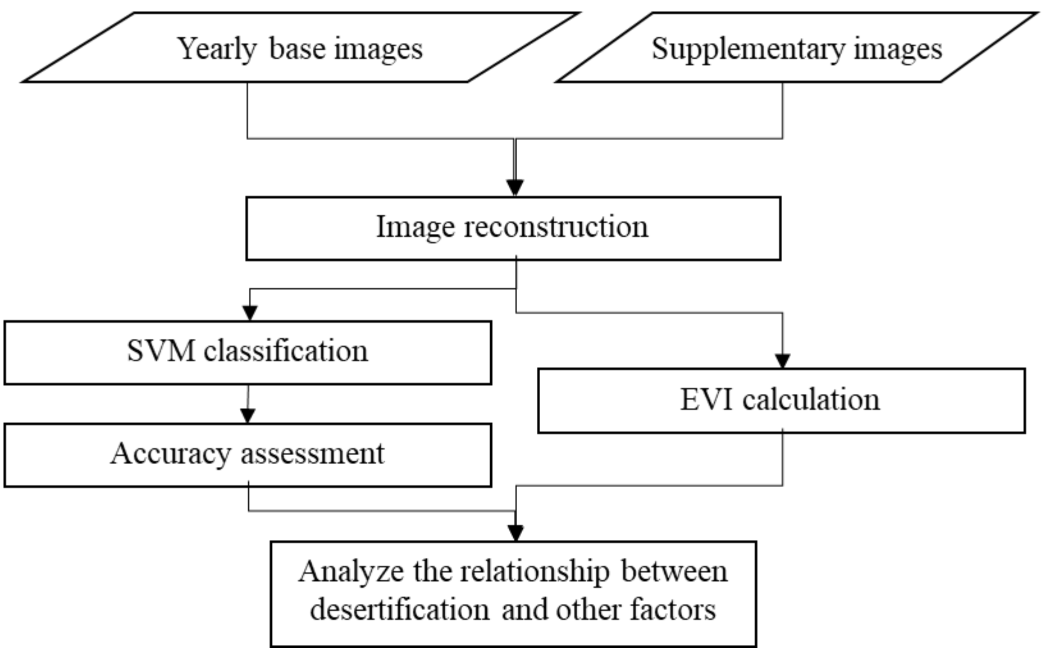

Figure 3. Flowchart of this study

Cloud- and gap-free image reconstruction

When composing a long-term Landsat image time series, it is inevitable that some images contain pixels contaminated by clouds and cloud shadows (Figure 4.a).

Additionally, Landsat 7 ETM+ images have a problem called Scan Line Corrector (SLC) failure after May 31, 2003. Without the compensation provided from SLC, the line of sight of ETM+ traces a zig-zag pattern along the satellite ground track. Because of the problem, there are approximately 22% of the pixels that cannot be scanned for each image (Figure 4.b). Therefore, these problematic pixels should be interpolated before the multiyear images are used to track the vegetation change. Otherwise, these images cannot be compared directly.

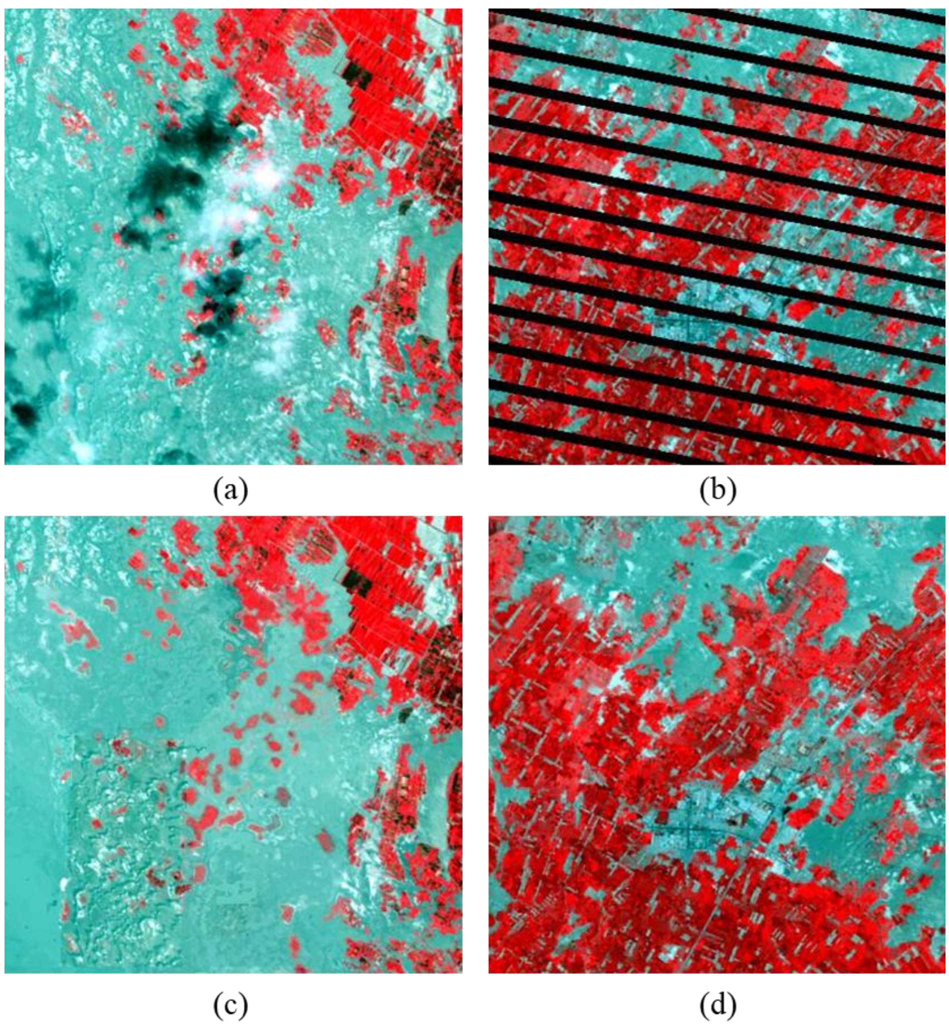

Figure 4. A Landsat 7 cloudy subimage in 2002 (a), a subimage with SLC-off gaps in

2007 (b). (c) and (d) are the reconstructed images of (a) and (b), respectively.

These problematic pixels can be interpolated by an advanced interpolator, Neighborhood Similar Pixel Interpolator (NSPI) (Chen et al., 2011; Zhu et al., 2012 a, b; Zhu et al., 2018). For the base images listed in Table 1, if the image has problematic pixels, additional images captured in the same year are also downloaded and used as ancillary data to interpolate the problematic pixels by the NSPI method. NSPI has been widely used and can obtain satisfactory results in many scenarios. Visual inspection of the reconstructed images also demonstrates that the problematic pixels were successfully recovered, as shown in Figure 4(c) and (d).

Vegetation cover and greenness extraction

Two methods are used to quantify the status of vegetation in Minqin County: hard classification and enhanced vegetation index (EVI). Hard classification assigns a class label (e.g., vegetation, water, soil, etc.) to each pixel (Tso & Mather, 2001). In this study, the Support Vector Machine is used to perform hard classification. SVM is a supervised classifier that can produce an optimal separating hyperplane to separate classes with the maximum distance among classes (Brereton & Lloyd, 2010). Considering that different desert types have very different spectral characteristics, the classification scheme includes vegetation, water, and four other desert types (sandy desert, Gobi desert, salinized land, and bare rock). These different desert types are grouped into one class in the subsequent analyses, including accuracy assessment and spatiotemporal analysis. The training samples were selected in the image of each year by visual interpretation with help from high-resolution images in Google Earth. The classification accuracy was assessed by confusion matrix and independent ground samples that were not used for training the SVM. The confusion matrix is used to describe the classification error for each class and errors related to incorrect classification (Congalton, 1991). Both overall accuracy and the Kappa coefficient derived from the confusion matrix were reported. In this study, the classification results are generally similar among years, so the classification accuracy assessment was done for images every five years instead of all images.

Hard classification has a large uncertainty for mixed pixels where pixels belong to multiple classes (Fisher & Pathirana, 1990; Foody, 1996). In the vegetation study, vegetation indices have been widely used to quantify the vegetation density and greenness in a pixel. In this study, EVI was used because it is better than other indices for vegetation monitoring through a decoupling of the canopy background signal and a reduction in atmosphere influences. EVI can be calculated using following equation:

$$EVI = G * \frac{(\rho_{NIR} - \rho_{RED})}{(\rho_{NIR} + C_1 * \rho_{RED} - C_2 * \rho_{BLUE} + L)}, \qquad (1)$$

where ρ is the land surface reflectance in the NIR (near infrared), red and blue bands, and G, C1, C2, and L are coefficients. For Landsat images, the coefficient C_1 is 6.0 and C_2 is 7.5. The soil adjustment factor L is 1.0 and the gain factor G is 2.5 (Jensen

2007). The value of EVI ranges from 0 to 1 (Sano et al., 2005). Compared with the Normalized Difference Vegetation Index (NDVI), EVI corrects the distortion caused by reflected light from particles in the air and from the ground below the vegetation. As shown in Figure 5, EVI can describe the greenness of the vegetation well. Vegetation pixels have much higher EVI values than other nonvegetation land covers such as desert, water and buildings.

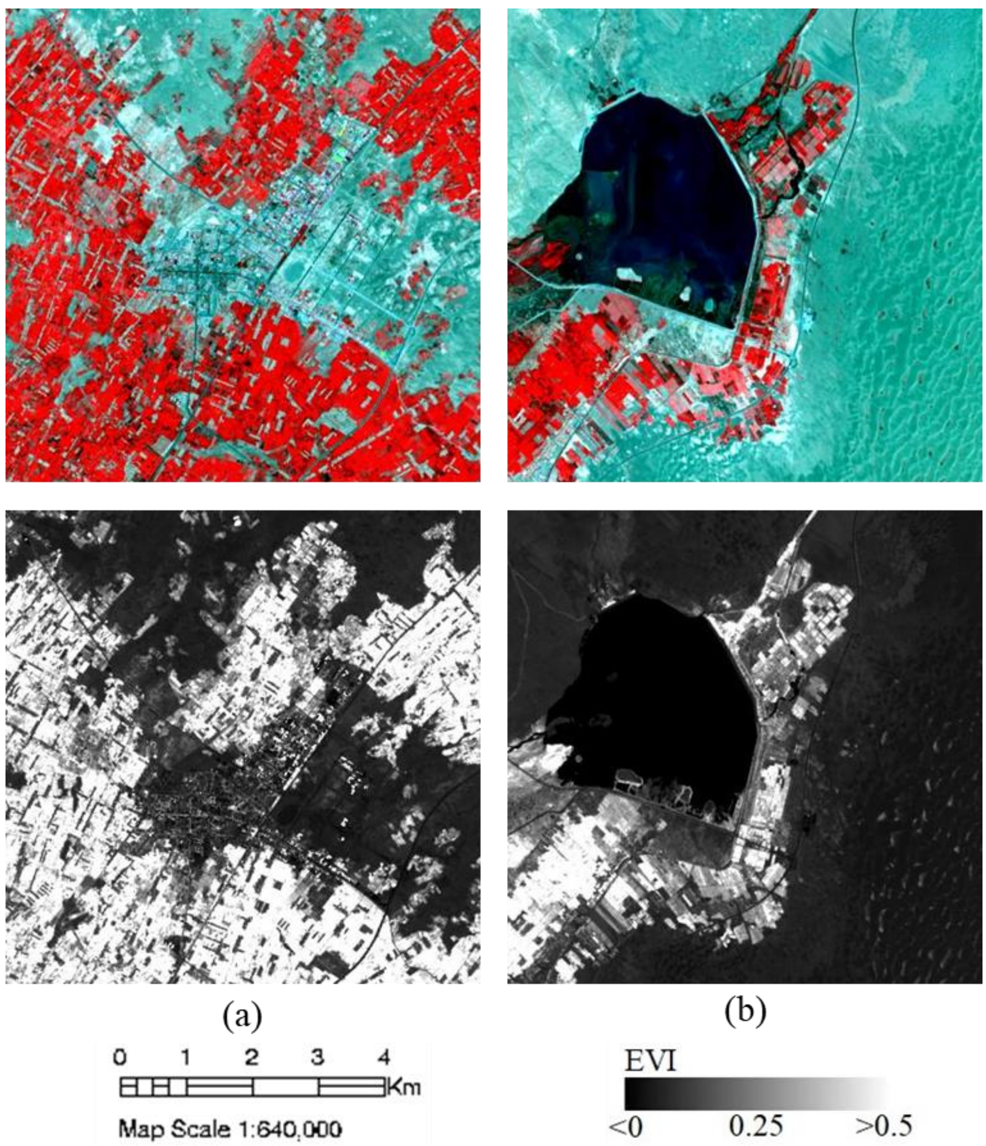

Figure 5. NIR-red-green composites of images (upper row) and EVI (lower row) of a subregion surrounding the county seat of Minqin (a) and a subregion surrounding a lake (b) in 2017.

All EVI images were stacked to compose a time series for all pixels. As EVI can represent the greenness of vegetation, if desertification happens, i.e., a vegetation pixel becomes desert over the 31 years, the curve of the EVI time series should have a descending trend. The stable desert area should have consistent and very low EVI values over the 31 years. Simple linear regression will be implemented to find the temporal trend of EVI values for each pixel. P-values of the simple linear regression were used to highlight the pixels with significant trends if their P-value was smaller than 0.05 (Greenland et al., 2016).

Results

Figure 6 shows the land cover classification of all years from 1987 to 2017. The accuracy assessment of selected images confirms that these classification results are reliable for further analysis, overall accuracy >94.7% and kappa> 0.927 (Table 2). Vegetation cover over all years distributes along the northeast-southwest direction, and vegetation pixels are clustered along this direction. The vegetation area is surrounded by deserts. The distribution of vegetation among all years is generally similar, but the distribution shows some variations in different years. From Figure 6, we can see that vegetation pixels increase gradually in these 31 years. The comparison between the land cover map of 1987 and 2017 shows a clear extension of the vegetation. The percentage of vegetation cover over the whole study area in each year also demonstrates this increasing trend (Figure 7). However, some years experienced vegetation loss in the past 31 years. From 2007 to 2013, the desertification became serious. The vegetation cover continues to decrease in these 7 years. After this period, desertification has been stopped, and the vegetation cover continues to increase to reach the percentage in 2006.

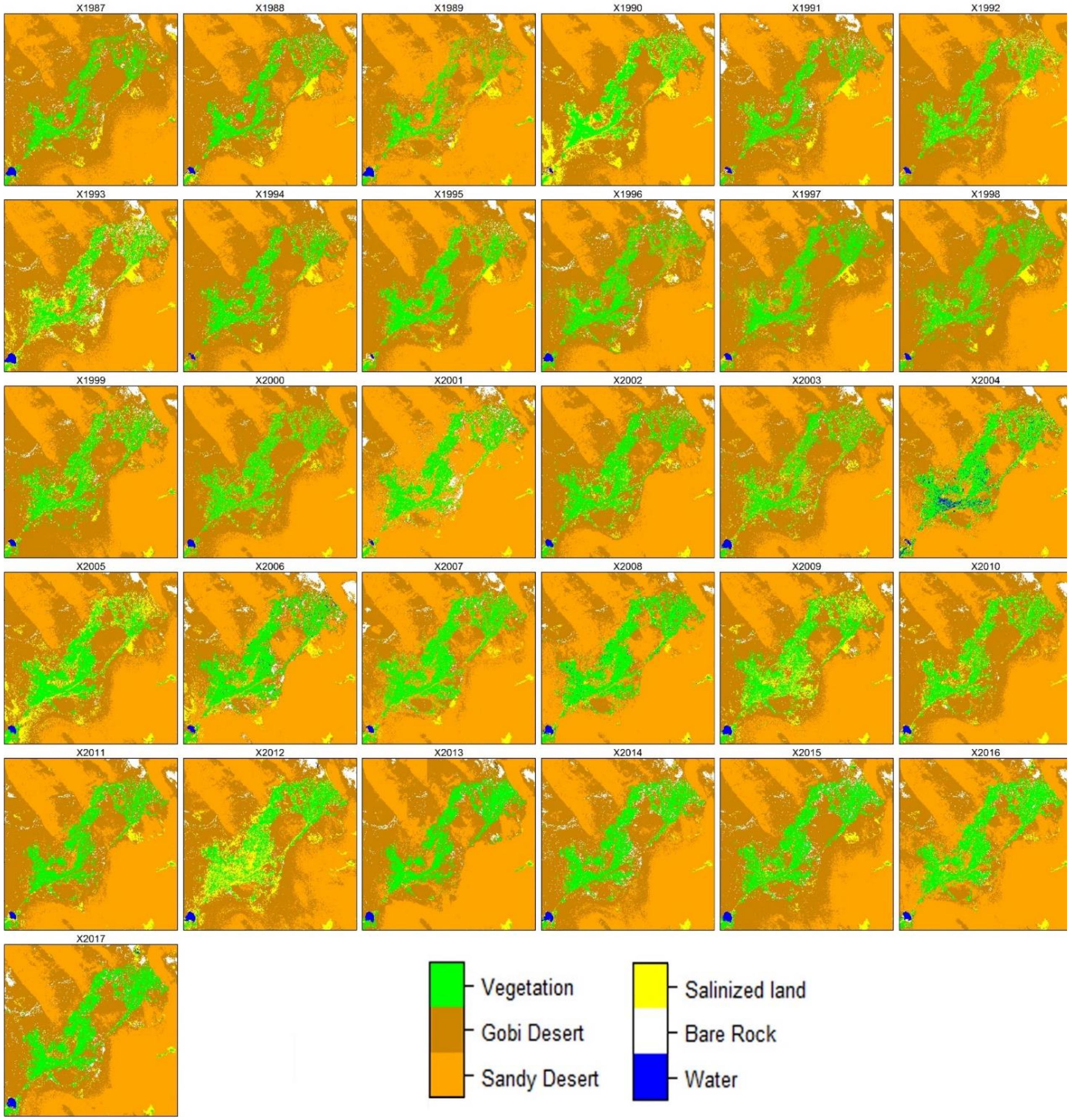

Figure 6. Classification results for each year in Minqin County from 1987 to 2017

Table 2. Accuracy assessment of classification results of selected images

Year	Overall Accuracy (%)	Kappa Value
1990	94.7276	0.9274
1995	99.5329	0.9629
2000	98.0844	0.8282
2005	98.2906	0.9659
2010	98.3189	0.9030
2015	99.5221	0.9443

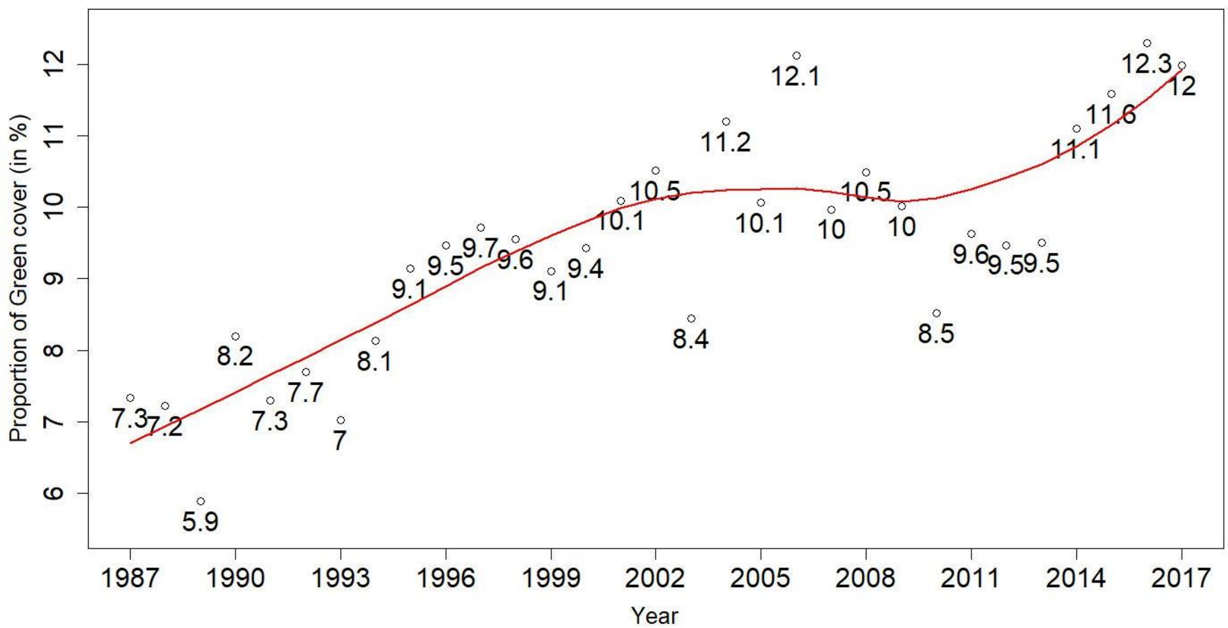

Figure 7. Vegetation cover percentage in Minqin County from 1987 to 2017. Red line is the moving average to show the trend

For each pixel in the study area, we can obtain the temporal change trend of EVI values over the 31 years by regressing EVI against years relabeled from 1987 (i.e., 1, 2, … as 1987, 1988, …) (Figure 8). From the temporal trend of EVI, there are 4 possible situations: (1) stable desert area with no change; (2) stable vegetation area with no change; (3) vegetation greenness increasing; and (4) vegetation greenness decreasing. In

Figure 8, the black region indicates that EVI changes are very small (change ranging from -0.1 to 0.1 over the 31 years) or not significant (P-value > 0.05). The green area is where the vegetation greenness becomes gradually better. These pixels may be threatened by desertification in some years but the overall trend over the 31 years is increasing vegetation. The red area is where vegetation has degraded over the 31 years. This scenario happens mainly in the region surrounding the urban area (marked by the circle in Figure 8) where intensive human activities exist. Another region surrounding the lake in the lower left of study area also experienced EVI decrease. Through inspecting the high-resolution images between 1984 and 2016, we found that the lake is extended so that vegetation pixels become water in this region. For the whole study area, the average EVI values of all pixels increased gradually over the 31 years (Figure 9), but with a short decreasing period from 2007 to 2013 that is consistent with the temporal trend of vegetation overage in Figure 7.

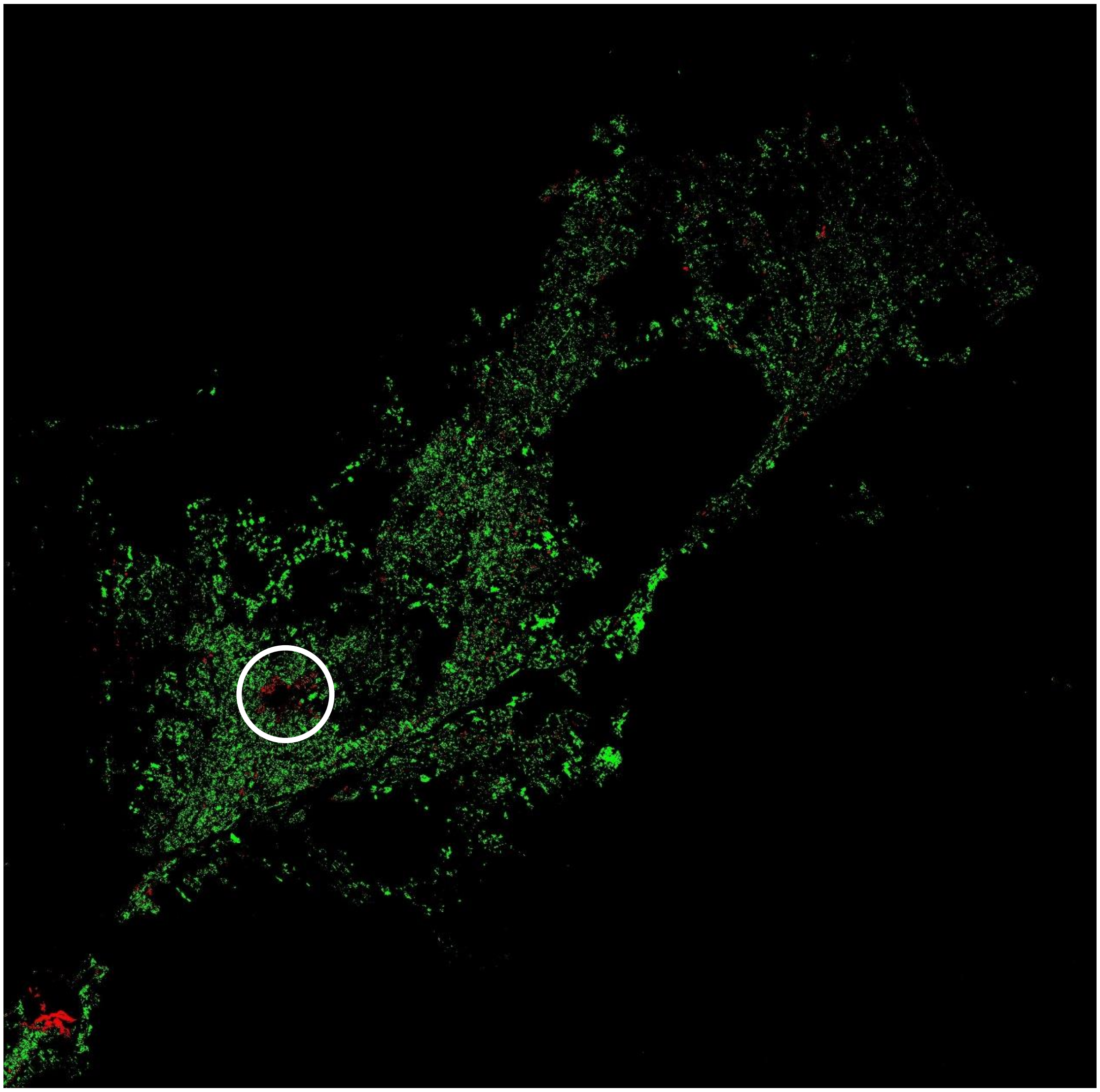

Figure 8. EVI temporal change over the past 31 years (green: EVI increasing, red: EVI decreasing). The circle marks the county seat.

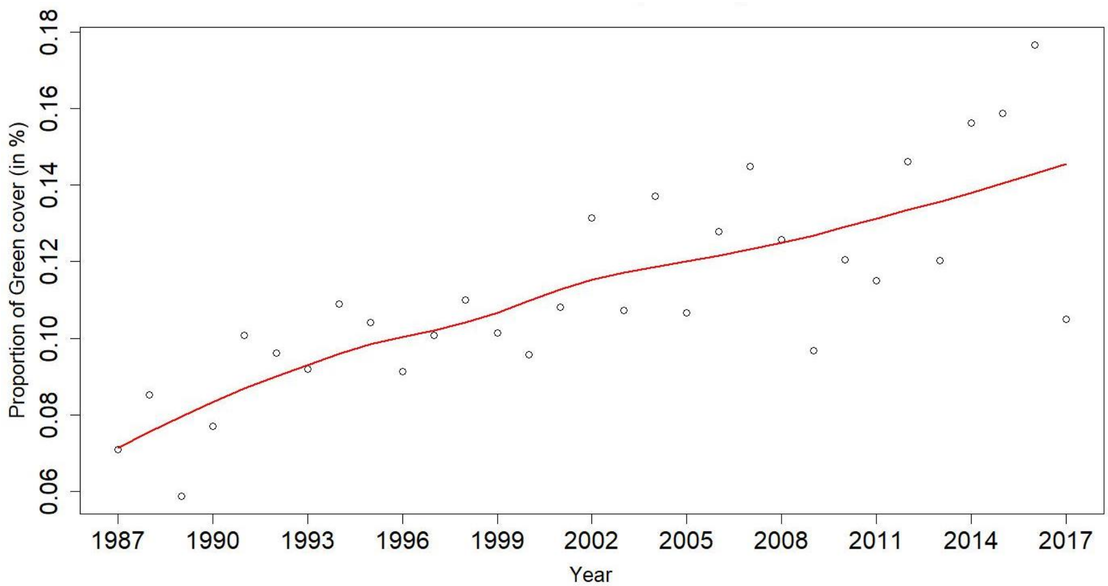

Figure 9. Mean EVI value of Minqin County from 1987 to 2017. Red line is the moving average to show the trend.

Discussion and Conclusions

According to the results, the vegetation cover of Minqin County is increasing during the study period, although some years have drops in vegetation cover and greenness. To explore the possible driving forces for these changes, both the climate and human factors were investigated.

Climate change, especially global warming and acidification, can increase evaporation of water and dry the soil, which, in turn, can decrease the vegetation cover and then cause land degradation. The geographic location is another nature factor associated with land degradation. Northwest China is located far from the sea, and the precipitation is low, erratic and concentrated mostly in the warmer months with high interannual variations. The low and irregular precipitation, along with Aeolian soil texture, erodible land surface, and strong and frequent winds, provides the dynamic force for soil erosion (Tao, 2014). Figures 10 and 11 show the temporal trend of annual average temperature and precipitation in Minqin County. The temperature in Minqin County is increasing from 1987 to 2013, while the precipitation shows no significant change trend. Given the annual change of temperature and precipitation, the study area should become gradually drier over the study period. Under this scenario, the desertification would become more serious. As the result, the vegetation coverage and greenness would have declined over the past 31 years. However, the Landsat EVI data show an increasing trend. Therefore, climate may not be the dominant factor influencing the vegetation in Minqin County from 1987 to 2017, or the negative effect of climate has been weakened by the governmental policies against desertification that will be discussed in the following paragraphs.

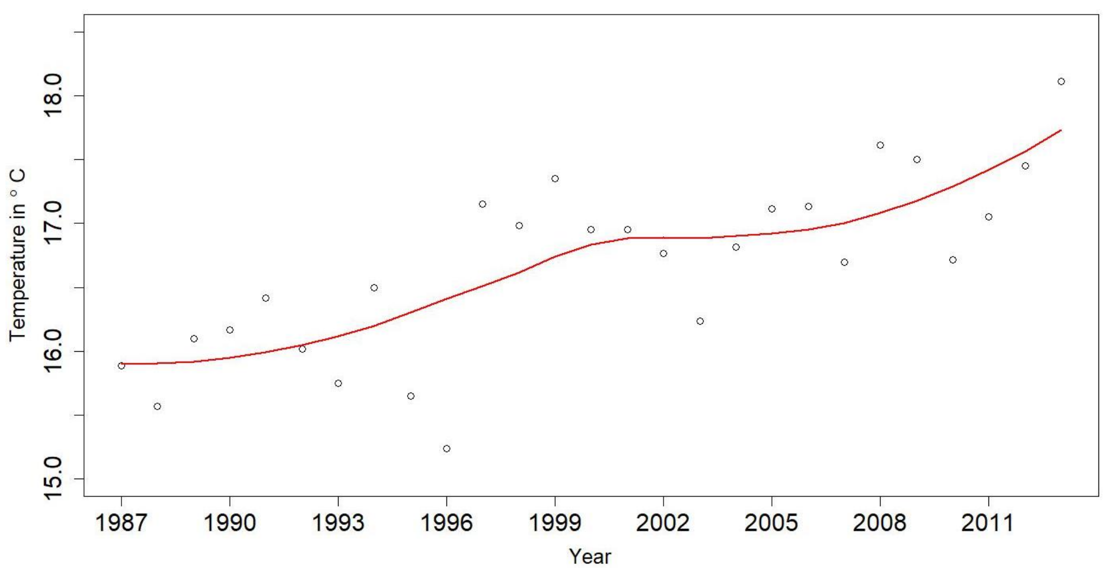

Figure 10. Annually average temperature in Minqin County from 1987 to 2013. Red line is the moving average to show the trend.

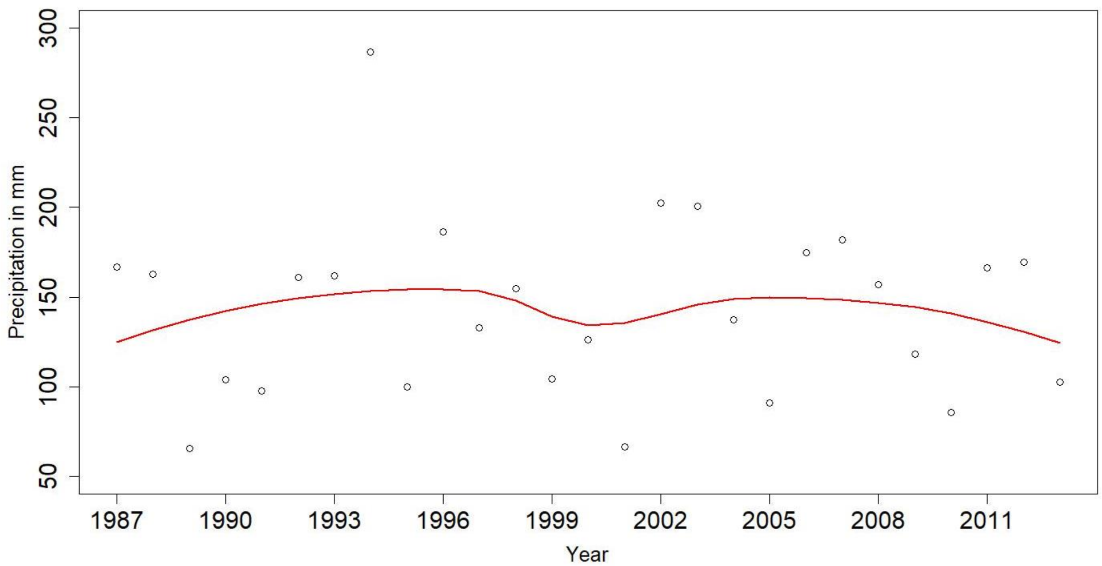

Figure 11. Annually average precipitation in Minqin County from 1987 to 2013. Red line is the moving average to show the trend.

In addition to nature factors, human activities can also speed up or slow down the desertification process (Tao, 2014). The increasing trend of vegetation coverage and greenness over the recent 31 years also suggests the effectiveness of policies from the Chinese Government for slowing down desertification. The state council of China proposed strategies for combating the desertification: (1) manage the Shiyang River sustainably; (2) protect the ecology and water; and (3) plant trees (Chang, 2008). This strategy gives the instructions to the local officers and citizens for defending against desertification.

Another important policy for combating desertification in Minqin County is implementing water-saving irrigated agriculture. From the high-resolution images in Google Earth, most of the vegetation areas in Minqin County are actually croplands. Groundwater is the major source for the irrigated agriculture. According to the data retrieved from a data sharing platform (tjsql.com), groundwater supply in Gansu province has dramatically decreased during 2007 to 2012 (Figure 12), which is well consistent with the drop of vegetation cover and greenness during this period (Figures 8 and 10). To reduce the water demand for irrigation, the planting of high water-consumption crops such as corn and onion has been limited (Ma et al., 2017). Some crops such as grape and jujube are perennial plants. The demand for fertilizer and water for the growth of these plants is lower than for other crops. In addition, the roots of these plants can grasp the soil to prevent soil erosion. Minqin County has high production of these plants. Thus, the government encourages the planting of grape and jujube and the relative food processing technologies such as intensive food processing and the wine-brewing industry (Pan et al., 2007).

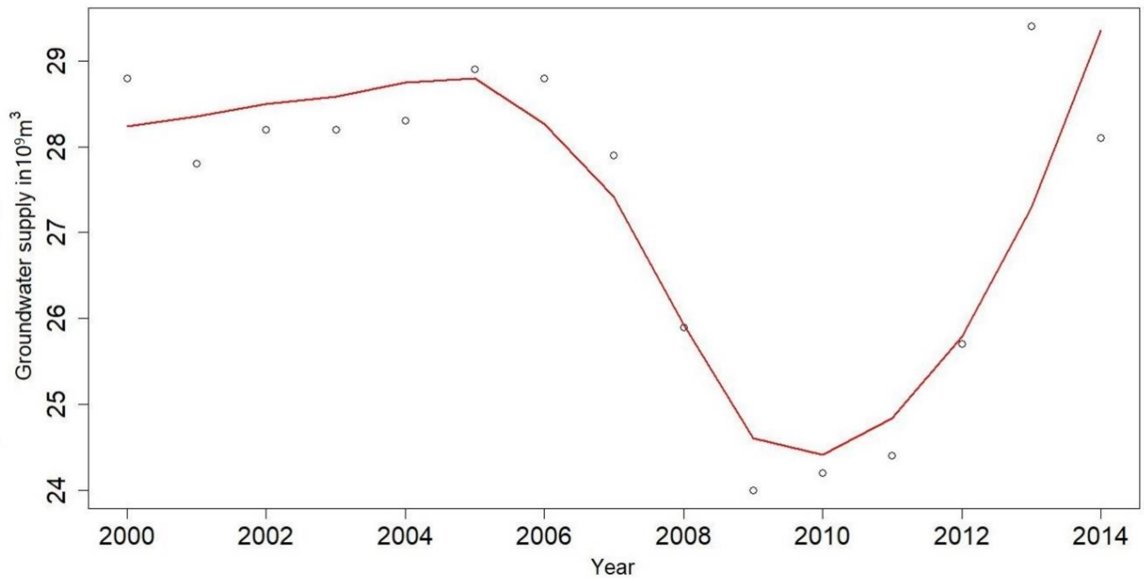

Figure 12. Groundwater supply in Gansu province from 2000 to 2014 derived from a data-sharing platform (tjsql.com)

Desertification is a global issue. Many countries are facing this problem. As a place that has been highly affected by desertification, Minqin County is an idea natural laboratory for studying the dynamic process of desertification and for investigating the effectiveness of policies aimed at slowing down desertification. This study is the first to use dense Landsat time series to assess the interannual vegetation coverage and greenness over a long period. The results of this study show that the desertification in Minqin County has temporally eased in recent years. For other places facing similar problems, Minqin County can be a positive example for mitigating desertification.

References

Brereton, R.G., Lloyd, G.R., 2010. Support Vector Machines for classification and regression. Analyst 135, 230–267. https://doi.org/10.1039/B918972F

Chang, Z., 2008. Study on Formation, Evolution and Sustainability of the Minqin Artificial Oasis. Arid Zone Research. 25, 1–9.

Chen, J., Zhu, X., Vogelmann, J. E., Gao, F., Jin, S. 2010. A simple and effective method for filling gaps in Landsat ETM+ SLC-off images. *Remote Sensing of Environment, 115*, 1053–1064.

Congalton, R.G., 1991. A review of assessing the accuracy of classifications of remotely sensed data. Remote Sens. Environ. 37 (1), 35–46.

Feng, L., Jia, Z., Li, Q., 2016. The dynamic monitoring of aeolian desertification land distribution and its response to climate change in northern China. Sci. Rep. https://doi.org/10.1038/srep39563

Fisher, P., & Pathirana, S. (1990). The evaluation of fuzzy membership of land cover classes in the suburban zone. Remote Sensing of Environment, 34(2), 121-132.

Foody, G.M., 1996. Approaches for the production and evaluation of fuzzy land cover classifications from remotely-sensed data. Int. J. Remote Sens. 17, 1317–1340. https://doi.org/10.1080/01431169608948706

Greenland, S., Senn, S.J., Rothman, K.J., Carlin, J.B., Poole, C., Goodman, S.N., Altman, D.G., 2016. Statistical tests, P values, confidence intervals, and power: a guide to misinterpretations. Eur. J. Epidemiol. 31, 337–350. https://doi.org/10.1007/s10654-016-0149-3

Guo, M., Li, X., 2005. Monitoring sandy desertification of Minqin oasis, northwest China by remote sensing and GIS. Int. Geosci. Remote Sens. Symp. 1, 206–209. https://doi.org/10.1109/IGARSS.2005.1526143

Jensen, J. (2007). Remote sensing of the environment: An earth resource perspective (2nd ed., Prentice Hall series in geographic information science). Upper Saddle River, NJ: Pearson Prentice Hall.

Li, M., Guo, P., Singh V.P., 2016. An efficient irrigation water allocation model under uncertainty. Agriculture Systems. 144, 46–57.

Liu, J., Li, S., Ouyang, Z., Tam, C., Chen, X., 2008. Ecological and socioeconomic effects of China’s policies for ecosystem services. Proceedings of the National Academy of Sciences. 28, 9477-9482.

Ma, J., Yan, Z., Fu, G., Liu, H., Yuan, H., Liu, S. 2017. Impacts of disposal projects on the groundwater level and degree of mineralization in the lower reaches of Shiyang River. Journal of Lanzhou University (Natural Science). 53, 489–493. https://doi.org/10.13885/j.issn.0455-2059.2017.04.008

Pan, J., Liu, P., Sun G., Bai, Y, Cheng,Y., 2007. Modern Agricultural Development Countermeasures in Minqin Oasis. Res. Agric. Mod. 28, 749–752.

Sano, E.E., Ferreira, L.G., Huete, A.R., Sano, E.E., Ferreira, L.G., Huete, A.R., 2005. Synthetic Aperture Radar (L band) and Optical Vegetation Indices for Discriminating the Brazilian Savanna Physiognomies: A Comparative Analysis. Earth Interact. 9, 1–15. https://doi.org/10.1175/EI117.1

Sun, D., 2015. Detection of dryland degradation using Landsat spectral unmixing remote sensing with syndrome concept in Minqin County, China. Int. J. Appl. Earth Obs. Geoinf. 41, 34–45. https://doi.org/10.1016/j.jag.2015.04.015

Sun, D., Dawson, R., Li, H., Li, B., 2005. Modeling desertification change in Minqin County, China. Environ. Monit. Assess. 108, 169–188. https://doi.org/10.1007/s10661-005-4221-9

Sun, D., Liu, N., 2015. Coupling spectral unmixing and multiseasonal remote sensing for temperate dryland land-use/land-cover mapping in Minqin County, China. Int. J. Remote Sens. 36, 3636–3658. https://doi.org/10.1080/01431161.2015.1047046

Tang, Z., An, H., Deng, L., Wang, Y., Zhu, G., Shangguan, Z., 2016. Effect of desertification on productivity in a desert steppe. Sci. Rep. 6, 27839. https://doi.org/10.1038/srep27839

Tao, W., 2014. Aeolian desertification and its control in Northern China. Int. Soil Water Conserv. Res. 2, 34–41.

TSO, B. and MATHER, P.M., 2001, Classification Methods for Remotely Sensed Data (NewYork: Taylor and Francis Inc).

Wang, H., Ren, J., Wang, L., et al. 2016. Study on the Changes of Land Use Based on TM in Minqin County. Geomatics ＆ Spat. Inf. Technol. 39, 99–101.

Wang F., Pan, X., Wang, D., Shen, C., Lu, Qi. 2013. Combating desertification in China: Past, present and future. Land Use Policy. 31, 311–313.

Wang, X., Dong, Z., Zhang, J., Liu, L., 2004. Modern dust storms in China: An overview. J. Arid Environ. https://doi.org/10.1016/j.jaridenv.2003.11.009

Zhou, W., Gang, C., Zhou, F., Li, J., Dong, X., Zhao, C., 2015. Quantitative assessment of the individual contribution of climate and human factors to desertification in northwest China using net primary productivity as an indicator. Ecol. Indic. https://doi.org/10.1016/j.ecolind.2014.08.043

Zhu, X., Gao, F., Liu, D., and Chen, J., 2012. A Modified Neighborhood Similar Pixel Interpolator Approach for Removing Thick Clouds in Landsat Images. IEEE Geoscience and Remote Sensing Letters 9(3):521–25.

Zhu, X., Helmer, E.H., Chen, J., Liu, D., 2018. An Automatic System for Reconstructing High-Quality Seasonal Landsat Time Series. In Weng Q (Eds.), Remote Sensing Time Series Image Processing (pp. 25-42). CRC Press.

Zhu, X., Liu, D., and Chen, J. 2012. A New Geostatistical Approach for Filling Gaps in Landsat ETM+ SLC-off Images. Remote Sensing of Environment 124:49–60.

Zucca, C., Della Peruta, R., Salvia, R., Sommer, S., Cherlet, M., 2011. Towards a World Desertification Atlas. Relating and selecting indicators and data sets to represent complex issues. Ecol. Indic. 15, 157–170. https://doi.org/10.1016/j.ecolind.2011.09.012